A REPORT ON THE INVESTIGATION OF THE AERODYNAMIC CHARACTERISTICS OF AN UNMANNED COMBAT AERIAL VEHICLE

BY

IBEMORAH ARINZE EMMANUEL

TABLE OF CONTENT

S

TABLE OF FIGURES

ABSTRACT

This report presents the findings of a comprehensive investigation into the non-linear aerodynamic characteristics of an Unmanned Combat Aerial Vehicle (UCAV). The study aimed to assess and understand the aerodynamic performance of the UCAV, and compare the different methods of analysis.

INTRODUCTION

The backbone of engineering is the strive to make improvements and innovative ways of doing things. This mindset has led to the development of high-speed aircraft which lead to focus on delta wings (Karthick Sk, 2021).

Phenomena such as highly swept wings and vortex-flow separation from sharp leading edges being of particular interest. These elements play a pivotal role in the design and performance of high-speed aircraft, where aerodynamic efficiency and stability are paramount.

Highly swept wings are wings that have a significant angle between the wing's leading edge and its direction of motion. Engineered for supersonic flight, they introduce intricate vortex flow patterns that have a profound impact on an aircraft's lift, drag, control, and stability.

The aim of this paper is to report an investigation into the non-linear aerodynamic behaviour associated with the separated-vortex flow from the highly swept sharp leading-edge wing.

Background

The principle of swept wings is to reduce wave drag over the wings by delaying the formation of shockwaves in transonic and supersonic flight (Aleks Udris, 2014).

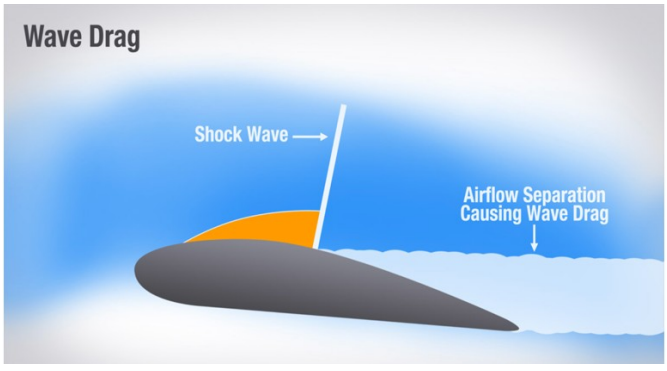

Figure 1: Flow separation due to wave drag. (BoldMethod, 2014)

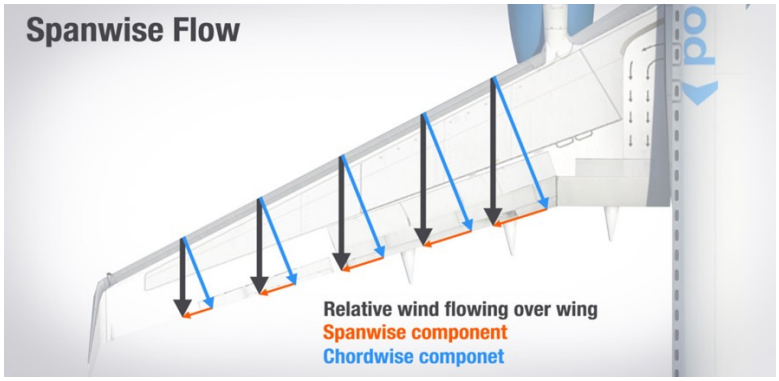

Figure 2: Airflow over a swept wing (BoldMethod, 2014)

Highly swept wings have benefits, but they are not without their disadvantages, with vortex-flow separation being a prominent issue (Henderson, 1976).

Vortex-flow separation from sharp leading edges is a phenomenon that occurs in highly swept wings, particularly in supersonic and transonic flight. The sharp leading edges of these wings create conditions where the airflow can separate from the wing's surface, leading to the formation of vortices. This separation results in reduced efficiency of the aircraft performance and safety, especially during manoeuvrers and at high angles of attack.

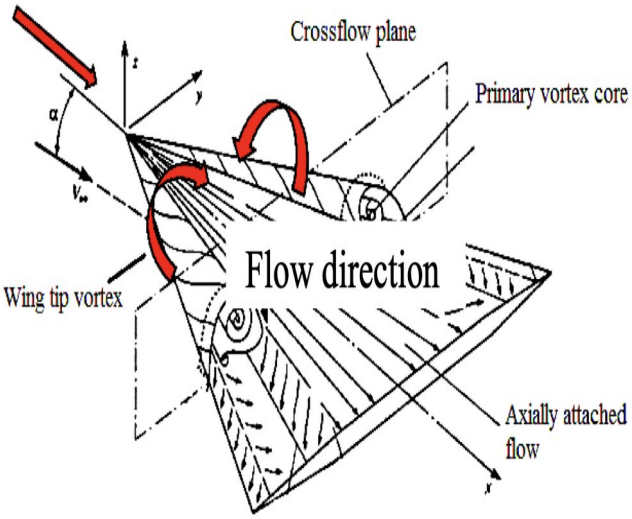

Figure 3: Flow over conventional Delta wing at certain angle of attack in subsonic condition. (Patil, 2021)

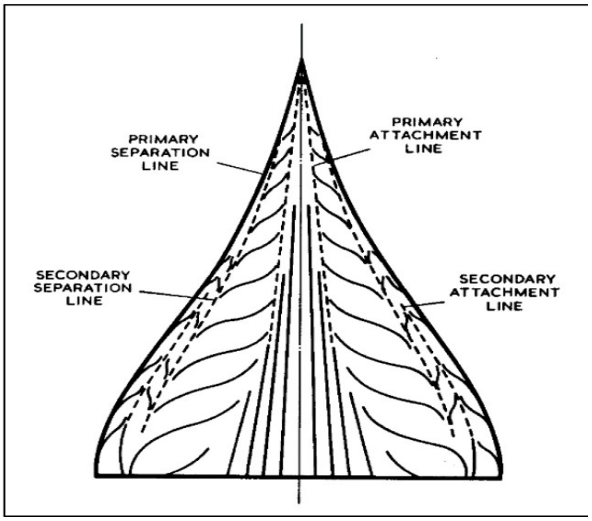

Figure 4: Illustration of surface friction lines due to separated flow vortex (Sugar-Gabor, 2023)

Analysing and predicting vortex-flow separation is a critical aspect of designing highly swept aircraft wings and understanding the non-linear aerodynamic behaviour, various techniques can be used, such as:

Computational Fluid Dynamics (CFD):

- CFD utilizes numerical simulations in predicting vortex-flow separation by analysing flow patterns and turbulence, aiding in a cost-effective way for wing design optimization.

Wind Tunnel Testing:

- Wind tunnel tests use scaled physical models to directly observe and measure the effects of vortex-flow separation on an aircraft's lift and drag these data serve as a crucial validation tool for CFD simulations and provide empirical data.

The CFD is one of the most effective methods because it is cost effective and saves time. They are different types of CFD methods like Vortex-lattice methods (VLM), etc.

The vortex lattice method is a numerical technique used in Computational Fluid Dynamics (CFD) to analyse the aerodynamic properties of aircraft wings and other lifting surfaces.

There are various approaches for solving the VLM like using a horseshoe vortex, or vortex rings.

In the vortex lattice method:

1. The wing's geometry is approximated by a series of flat panels, and thickness is assumed to be zero.

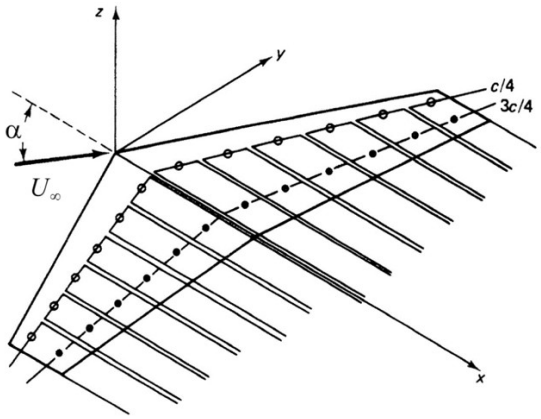

Figure 5: Control points and one Horseshoe vortex along chordwise direction (Sugar-Gabor, 2023)

2. Horseshoe vortices and control points are placed on these panels.

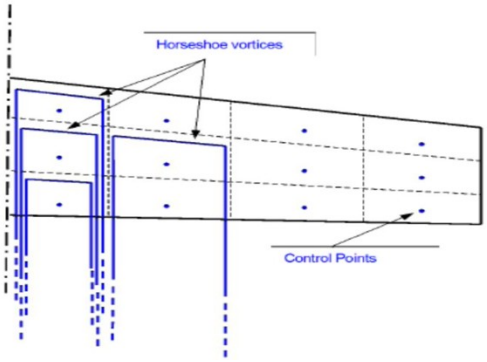

Figure 6: Trailing segments of horseshoe vortex superposed. (Sugar-Gabor, 2023)

3. The downward wash induced velocities at each panel's control points due to all the other vortices are calculated using the Biot-Savart law.

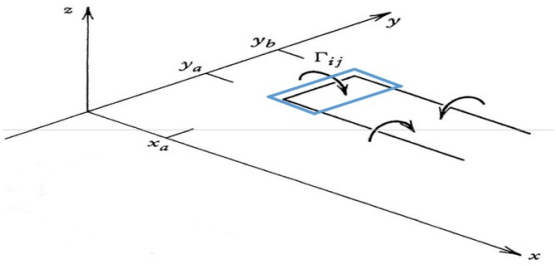

Figure 7: Horseshoe vortex with displayed strength $\Gamma_{(i,j)}$ bound to panel (i, j) (Sugar-Gabor, 2023)

4. The resulting velocities are used to compute the lift and other aerodynamic properties of the wing.

Here's a brief mathematical description of the Horseshoe vortex lattice method with equations:

Horseshoe Vortex Lattice Method Equations:

1. Induced Velocity at a Point (Vi):

The induced velocity at a point in space due to a vortex segment is calculated using Biot-Savart law for line vortices (Biot-savart, 1861):

$$w_{i,j}(x_c y_c)=\frac{1}{4\pi}\frac{1}{y_c-y_a}\left[1+\frac{\sqrt{(x_c-x_a)^2+(y_c-y_a)^2}}{x_c-x_a}\right]-\frac{1}{4\pi}\frac{1}{y_c-y_b}\left[1+\frac{\sqrt{(x_c-x_a)^2+(y_c-y_b)^2}}{x_c-x_a}\right] \text{for } x_c\neq x_a$$

$$\frac{1}{4\pi}\frac{1}{y_c-y_a}-\frac{1}{4\pi}\frac{1}{y_c-y_b} \text{for } x_c\neq x_a$$

It is assumed that the velocities at the control points are equal to the sum between the freestream velocity and the velocities induced by horseshoe vortices and the normal component of the velocity is zero.

$$U_\infty \sin\alpha-\sum_{k=1}^{N_x}\times\sum_{l=1}^{N_y}\Gamma_{k,l}W_{k,l}(x_c,y_c)_{i,j}=0$$

A linear system of $N=N_x\times N_y$ equations is obtained, and is solved to obtain the unknown vortex strength: $A_{N,N}\Gamma_N=b_N$

Kutta-Joukowski theorem is used to determine the lift force on panel (i,j) $L_{i,j}=\rho U_\infty \Gamma_{i,j}\Delta y$

The induced drag on panel (i,j) *is calculated by*: $D_{i,j}=\rho w_{1/4}\Gamma_{i,j}\Delta y$

To calculate induced drag calculation at the downwash at the $1/4$ chord point of the panel is needed: $w_{1/4}=\sum_{1,j}\Gamma_{i,j}w_{i,j}(x_{1/4},y_{1/4})$

VLM solvers can also be used, VLM solvers like XFLR depend on number of panels on the grid.

VLM grid Sensitivity Analysis:

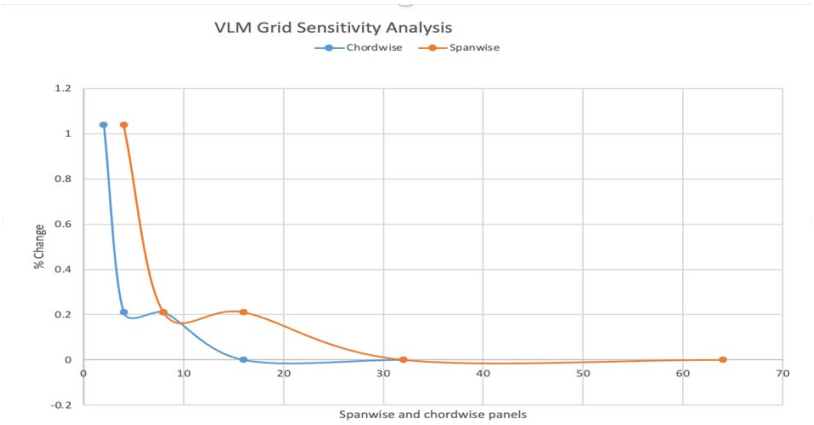

Figure 8: VLM Grid Sensitivity analysis

A grid sensitivity analysis was carried out in this experiment using factors of two in both chordwise and spanwise panels the result shows that at 32spanwise panels the percentage change became zero and at 18 chordwise panels the percentage change was also zero, this shows that any grid above 18 chordwise and 32spanwise panels would give correct answer.

METHODOLOGY

Data for the experiment was gotten using a No. 1 Closed return Low-speed Wind tunnel with working section dimensions of 1.14m width and 0.82m height, giving the wind tunnel a cross sectional area of 0.9348m^2. Lift forces, drag forces, and pitching moments are measured over different angles.

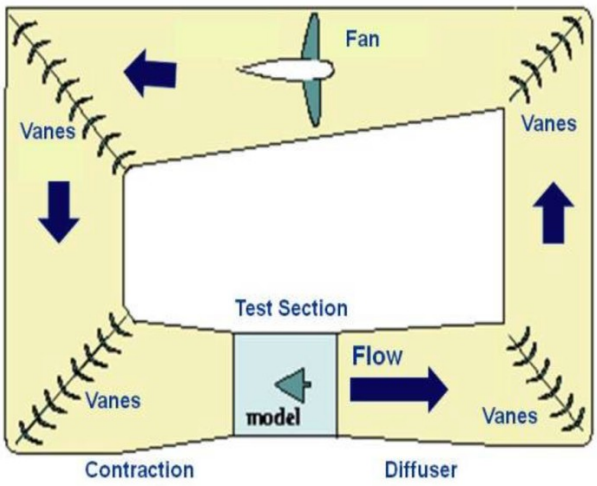

Figure 9: Diagram showing parts of the test equipment.

Figure 10: No. 1 Closed Return Low-speed wind tunnel

The forces and moments are measured with loads balance installed above the test section; model is attached via support rods. The balance uses linear variable differential transformers (LVDTs) to measure the output which is in microvolts(mV). Dynamic pressure is measured by Betz manometer.

The experimental procedure is outlined as follows:

1. With the model set at a zero angle of attack and the wind tunnel turned off, voltage outputs from the load cells for lift, drag, and pitching moment are recorded. These initial readings, termed wind-off values, serve as reference values and are subtracted from subsequent measurements.
2. The wind tunnel is activated, and the flow is set to a speed of 500, corresponding to 50% power. The system is allowed to stabilize, with particular attention to the Betz manometer reading to ensure steady flow conditions.
3. The model is pitched to an angle of attack of -10 degrees (where negative angle corresponds to positive pitch). Voltage outputs for lift, drag, and pitching moment are recorded, along with the Betz manometer reading in millibars (mbar).
4. In increments of 2 degrees in angle of attack, measurements are repeated for each setting, including voltage outputs and the Betz manometer reading, until a maximum angle of attack of +26 degrees is reached.
5. To account for environmental conditions, atmospheric pressure and temperature readings are taken using a digital barometer and thermometer available in the laboratory. These measurements contribute to the overall data collection process for the experiments.

The data was processed in the following ways:

1. The readings were all collated and average values gotten for each angle of attack and the wind off values were then subtracted.
2. The values gotten are now converted from millivolts to newton and newton meters respectively by multiplying by conversion factors, then the dynamic pressure calculated using manometer reading, then aerodynamic coefficients were obtained using the converted forces and moments, then the measured angles of attack and drag coefficients are corrected using the calculated Oswald's efficiency then density, viscosity and other important values are gotten.
3. Then XFLR was used to simulate the same experiment assuming of an inviscid flow and the values gotten were exported to an excel sheet.
4. Then the non-aerodynamic coefficient that account for the polhamus suction analogy were calculated.

5. Then values were plotted against each other to understand the reliability of the individual methods.

RESULTS

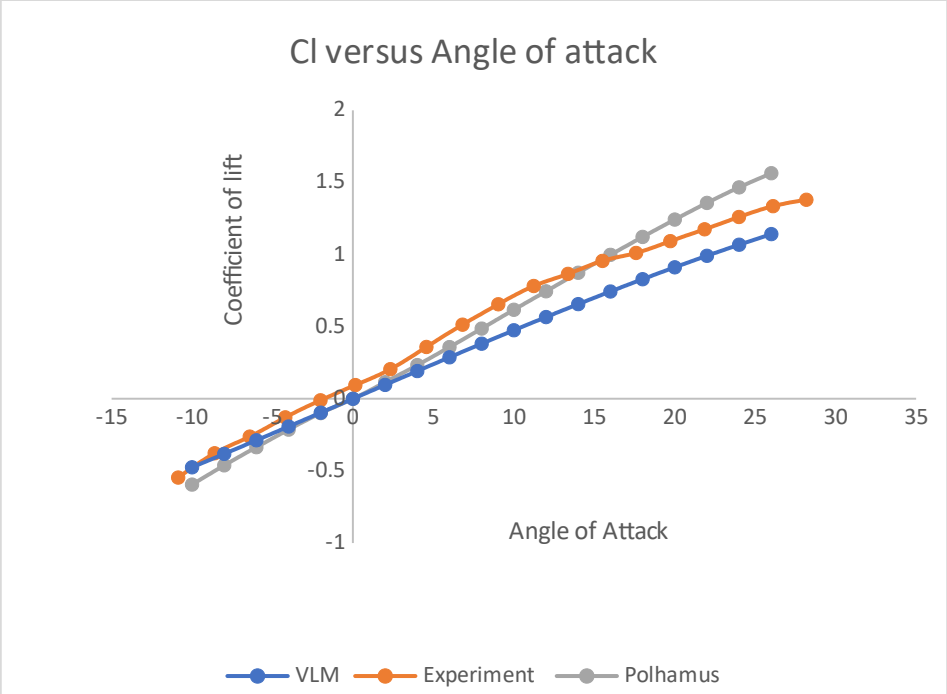

Figure 11: Graph of Coefficient of Lift against Angle of attack

From figure 11 above it can be visualized that as the angle of attack increased the lift generated also increased in the graphs above. But on further analysis of the figure 11 it is observed that the experimental is at a higher angle of attack because it was corrected due to strut used to attach the model affecting angles, and the VLM plot is a linear graph as a result of the assumption of an inviscid flow, the polhamus plot shows higher coefficient of lift because other effects were included in the calculations such as pitching moment, Rolling moment coefficient.

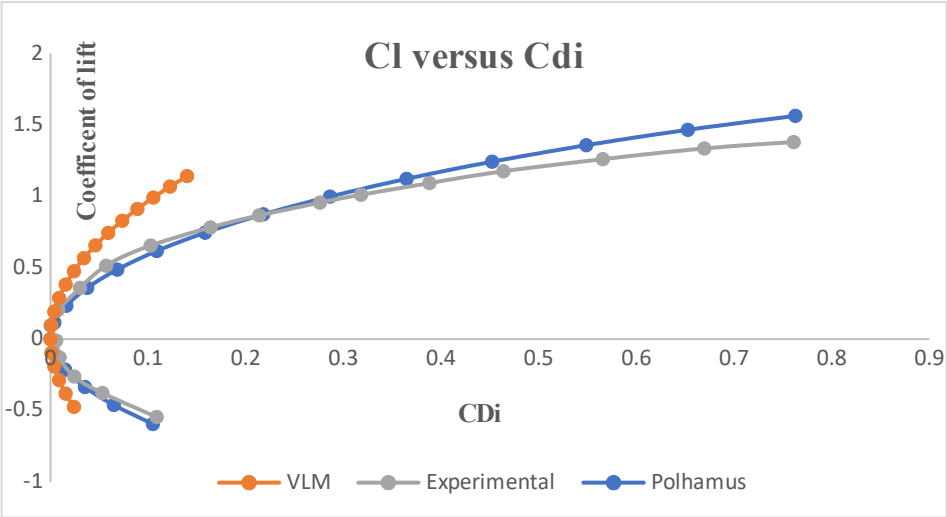

Figure 12: Graph of coefficient of lift against Induced drag

From figure 12 it can be observed that the graphs are of a parabolic nature, but the VLM values gotten from XFLR is less parabolic because of the assumption of an inviscid flow, the polhamus is of a higher coefficient of lift and the experimental has a higher coefficient of induced graph because of the supporting rods attached to the model thereby increasing the induced drag on the model.

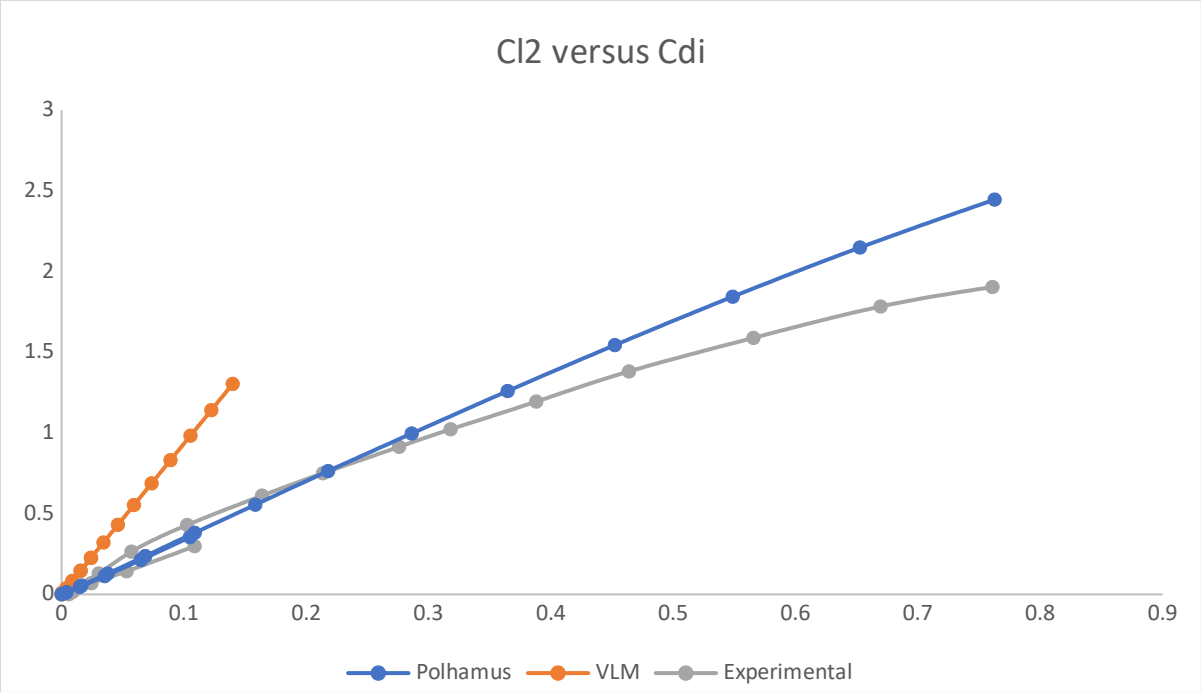

Figure 13: Graph of Cl^2 vs CD_i

Figure 13 explains figure 12 further by making the coefficient of lift all positive values by squaring it as that is more likely real-life experience.

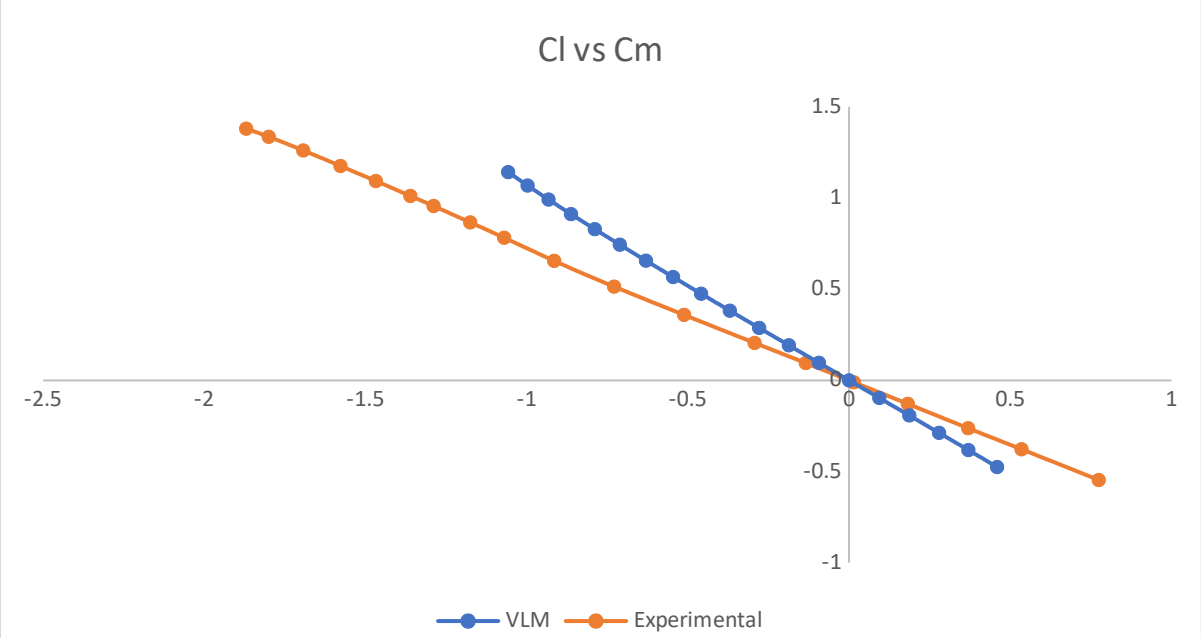

Figure 14: Graph of Cl versus Cm

From figure 14 it can be observed that the coefficient of lift and the coefficient of moment are inversely proportional on both graphs as the coefficient of lift increases the coefficient of moment reduces. The graph of experimental has a higher coefficient of moment than that of the VLM values gotten from XFLR this is due to assumptions in the program solvers.

DISCUSSION

From the graphs the experimental method is the most accurate but errors due to the support rods contribute to additional drag on the model.
The values gotten from the VLM solver XFLR is a bit off from the others and so is the least reliable due to the assumption and approximations done.
The polhamus analogy is reliable as it takes into consideration the wing and wake induced flows along the leading edge but it doesn't calculate the coefficient of moment as it would require a bit of modification of the distribution of the chord and an accurate prediction of the distribution of the vortex lift (Polhamus, 1966)

CONCLUSION

VLM solvers like XFLR are valuable for initial aerodynamic analysis and design, they make certain simplifications and assumptions that may not fully capture the intricacies of real-world aerodynamics. While Polhamus suction analogy takes into consideration all the interacting effects it still is a simplified version, Experimental results, on the other hand, provide a more direct and comprehensive view of aerodynamic behaviour but can also be influenced by various factors within the test apparatus and other uncertainties.

REFERENCE

5. Aleks Udris, 2014. *BoldMethod.* [Online]
   Available at: https://www.boldmethod.com/learn-to-fly/aerodynamics/wing-sweep/
   [Accessed 25 10 2023].
6. Biot-savart, 1861. *Wikepedia.* [Online]
   Available at: https://en.wikipedia.org/wiki/Biot–Savart_law
   [Accessed 26 10 2023].
7. BoldMethod, 2014. *Bold Method.* [Online]
   Available at: https://www.boldmethod.com
   [Accessed 25 10 2023].
8. Henderson, W. P., 1976. *EFFECTS OF WING LEADING-EDGE RADIUS AND REYNOLDS NUMBER ON LONGITUDINAL AERODYNAMIC CHARACTERISTICS OF HIGHLY SWEPT WING-BODY CONFIGURATIONS AT SUBSONIC SPEEDS,* WASHINGTON, D. C.: NATIONAL AERONAUTICS AND SPACE ADMINISTRATION.
9. Karthick Sk, D. S. S. D. J. C., 2021. Unsteadiness in a leading-edge separated flow at supersonic speed. *APS Division of Fluid Dynamics Meeting Abstracts,* E03.(00), pp. 3-6.
10. Patil, M., 2021. Effect of Vortex Generator on the Flow Field over a Conventional Delta Wing in Subsonic Flow Condition at Higher Angles of Attack. *Faculty of Mechanical Engineering, Belgrade.,* 49(2), pp. 395-400.
11. Polhamus, E., 1966. *A CONCEPT OF THE VORTEX LIFT OF SHARP-EDGE DELTA WINGS BASED ON A LEADING-EDGE-SUCTION ANALOGY,* Washington DC: National Aeronautics and space adminstration.
12. Smith, B. a., 1966. *Aerodynamics for Engineering Students.* [Online]
    Available at:
    http://www-mdp.eng.cam.ac.uk/web/library/enginfo/aerothermal_dvd_only/aero/vlm/vlm.html
    [Accessed 25 October 2023].
13. Smith, B. a., 2006. *Aerodynamics for Engineering Students.* [Online]
    Available at:
    http://www-mdp.eng.cam.ac.uk/web/library/enginfo/aerothermal_dvd_only/aero/vlm/vlm.html
    [Accessed 27 10 2023].
14. Sugar-Gabor, D. O., 2023. *Aerodynamics Lecture Notes,* Manchester : Salford University.
15. Sugar-Gabor, D. O., 2023. *Assesment Information ,* Salford: Salford University.

APPENDIX

Cl of Polhamus	-0.594853574	-0.461476722	-0.33569438	-0.2138126	-0.0992113	0	0.11490652	0.23349804	0.35840564	0.48685533	0.61715502	0.74510012	0.87380358	0.9980651	1.12225227	1.24258705	1.35789508	1.4658033	1.56382837
Cd of Polhamus	0.104888735	0.064856324	0.035282901	0.01495123	0.00346453	0	0.00401262	0.01632777	0.03766995	0.06842305	0.10882108	0.15837592	0.2178637	0.28619056	0.36464187	0.4522647	0.54862523	0.65261767	0.76273006
Cl2 of Polhamus	0.353850775	0.212960765	0.112690717	0.04571582	0.00984288	0	0.01320351	0.05452134	0.12845461	0.23702811	0.38088032	0.55517419	0.7635327	0.99613395	1.25945015	1.54402257	1.84387906	2.14857931	2.44555918

Figure 15: Data of Polhamus suction analogy

ANGLE OF ATTACK	-10	-8	-6	-4	-2	0	2	4	6	8	10	12	14	16	18	20	22	24	26
Coefficenet of Lift(Cl)	-0.4750384	-0.3819427	-0.2875797	-0.192257	-0.0962902	0	0.09629022	0.192257	0.2875797	0.3819427	0.4750384	0.5665696	0.6562515	0.7438147	0.8290064	0.911593	0.9913615	1.068121	1.141704
Coefficenet of Drag(Cd)	0.02405001	0.01553412	0.008800488	0.00393127	0.00098582	0	0.00098582	0.00393127	0.00880049	0.01553412	0.02405001	0.03424408	0.04599152	0.05914814	0.07355198	0.0890251	0.1053756	0.1223996	0.1398838
Coefficent Pitching Moment(Cm)	0.4589642	0.3698837	0.2790012	0.1867594	0.09360773	0	-0.0936077	-0.1867594	-0.2790012	-0.3698837	-0.4589642	-0.5458087	-0.6299941	-0.7111102	-0.7887618	-0.8625706	-0.9321771	-0.9972422	-1.057449
Coefficenet of Drag Induced(Cdi)	0.02405001	0.01553412	0.008800488	0.00393127	0.00098582	0	0.00098582	0.00393127	0.00880049	0.01553412	0.02405001	0.03424408	0.04599152	0.05914814	0.07355198	0.0890251	0.1053756	0.1223996	0.1398838
Coefficenet of Lift(Cl2)	0.225661481	0.145880226	0.082702084	0.03696275	0.00927181	0	0.00927181	0.03696275	0.08270208	0.14588023	0.22566148	0.32100111	0.43066603	0.55326031	0.68725161	0.8310018	0.98279762	1.14088247	1.30348802

Figure 16:Data from xflr

ANGLE OF ATTACK	-10	-8	-6	-4	-2	0	2	4	6	8	10	12	14	16	18	20	22	24	26
LIFT(mV)	-94.82275	-66.1553	-45.8519	-22.59075	-1.8428	16.7115	36.15715	62.5729	89.54935	113.3771	133.816	147.65425	162.3874	171.77225	184.9564	198.15945	212.5403	223.50425	229.2229
DRAG(mV)	213.9039	164.37425	137.5499	124.094	121.2793	115.38965	123.1282	142.48625	167.10065	207.5534	260.67115	304.55935	359.35745	397.11535	458.2827	524.0994	614.74815	702.12965	777.1652
Pitching Moment(mV)	151.47475	104.25105	67.8056	35.34245	2.9611	-25.0067	-62.21935	-105.7943	-143.6574	-150.0151	-130.4003	-122.9645	-117.26905	-119.00085	-121.8629	-128.9108	-140.4162	-161.03175	-186.2195
LIFT(N)	-37.4739508	-26.14457456	-18.120671	-8.9278644	-0.7282746	6.6043848	14.2893057	24.7288101	35.3899031	44.8066299	52.8840832	58.3529596	64.1755005	67.8843932	73.0947693	78.3126146	83.9959266	88.3288796	90.5888901
DRAG(N)	16.00001172	12.2951939	10.2887325	9.2822312	9.07169164	8.63114582	9.20998936	10.6579715	12.4991286	15.5249943	19.498202	22.7810394	26.8799373	29.7042282	34.279546	39.2026351	45.9831616	52.5192978	58.131957
Pitching moment(Nm)	1.6359273	1.12591134	0.73230048	0.38169846	0.03197988	-0.2700724	-0.671969	-1.1425784	-1.5514999	-1.6201631	-1.4083232	-1.3280166	-1.2665057	-1.2852092	-1.3161193	-1.3922366	-1.516495	-1.7391429	-2.0111706
Betz Manometer Reading	27.8	28.05	28	28.1	28.2	28.1	28.2	27.9	27.9	27.7	27.4	27.3	27.2	27.2	27.1	27	27	26.8	26.6
Dynamic Pressure(q)	319.85568	322.73208	322.1568	323.30736	324.45792	323.30736	324.45792	321.00624	321.00624	318.70512	315.25344	314.10288	312.95232	312.95232	311.80176	310.6512	310.6512	308.35008	306.04896
Coefficent of lift(CL)	-0.546144578	-0.377634491	-0.2622039	-0.1287254	-0.0104633	0.09522456	0.20529811	0.35910542	0.51392307	0.65536833	0.78198308	0.86601055	0.95592386	1.01116954	1.09279814	1.17514349	1.26042614	1.33533695	1.37980032
Coefficent of Drag(Cd)	0.233183837	0.177592842	0.14887672	0.13383478	0.13033532	0.12444718	0.13232228	0.15477232	0.18150913	0.22707777	0.2883148	0.33809117	0.40038914	0.44245826	0.51249391	0.58826693	0.69001416	0.79397542	0.88543411
Coefficent of Moment(Cm)	0.774215591	0.534687427	0.36922919	0.18214403	0.01484061	-0.1342259	-0.2930428	-0.5117298	-0.7288149	-0.9147704	-1.0698401	-1.1750513	-1.2886494	-1.3607647	-1.4676713	-1.5774864	-1.6929809	-1.7999465	-1.8699546
Coefficent of lift(CL^2)	0.2982739	0.142607809	0.0687509	0.01657023	0.00010948	0.00906772	0.04214732	0.1289567	0.26411692	0.42950765	0.61149754	0.74997427	0.91379042	1.02246383	1.19420779	1.38096223	1.58867405	1.78312478	1.90384893
Lift Induced drag Coefficent	0.108736653	0.053145658	0.02442953	0.0093876	0.00588813	0	0.00787509	0.03032514	0.05706195	0.10263059	0.16386762	0.21364399	0.27594195	0.31801108	0.38804673	0.46381975	0.56556698	0.66952824	0.76098692
Oswald's Efficency	-0.015039658	-0.010399249	-0.0072205	-0.0035448	-0.0002881	0.00262228	0.00565347	0.009889	0.01415235	0.01804745	0.02153415	0.02384809	0.02632411	0.02784545	0.03009333	0.03236095	0.03470945	0.03677233	0.03799676
Angle in radians	-0.174532925	-0.13962634	-0.1047198	-0.0698132	-0.0349066	0	0.03490659	0.06981317	0.10471976	0.13962634	0.17453293	0.20943951	0.2443461	0.27925268	0.31415927	0.34906585	0.38397244	0.41887902	0.45378561
Corrected Angle(Alpha)	-0.189572583	-0.150025589	-0.1119403	-0.073358	-0.0351947	0.00262228	0.04056006	0.07970217	0.1188721	0.15767379	0.19606707	0.2332876	0.2706702	0.30709813	0.3442526	0.3814268	0.41868189	0.45565135	0.49178237
Corrected Coefficient of Drag(Cd)	0.116950481	0.057072773	0.02632279	0.00984391	0.00589115	0.00024971	0.00903574	0.03387633	0.06433516	0.11445831	0.18070696	0.23429668	0.30110579	0.34616755	0.42093267	0.50184851	0.60931568	0.71863169	0.81341487
Corrected Angle(Alpha)Deg	-10.86170892	-8.595833088	-6.4137063	-4.2031034	-2.016509	0.15024567	2.32392012	4.56659785	6.8108697	9.03404256	11.2338158	13.3663946	15.5082602	17.595427	19.7242209	21.8541457	23.988705	26.1068996	28.177054
Velocity	23.26433169	23.36870337	23.3478664	23.3895218	23.4311032	23.3895218	23.4311032	23.3061365	23.3061365	23.2224517	23.096356	23.0541708	23.0119083	23.0119083	22.9695681	22.9271496	22.9271496	22.8420764	22.7566852
Reynolds	514450.3542	516758.3531	516297.579	517218.717	518138.218	517218.717	518138.218	515374.794	515374.794	513524.25	510735.863	509803.011	508868.449	508868.449	507932.168	506994.158	506994.158	505112.911	503224.632

Figure 17: Experimental Datasheet

Pressure	1008	mbar	100800	Pascals
Temp	24	deg C	297.15	Kelvin
Density	1.18196033			
Viscosity	1.83869E-05			
Cmac	0.344			
Kp	2.721769543			
Kl	0.107029381			
Lambda Leading edge	47.872			
Kv	2.875557506			

Figure 18: Data for Constants

X Plane	2	4	8	16	32
Y Plane	4	8	16	32	64
Cl	0.481	0.476	0.475	0.474	0.474
Cd	0.024	0.024	0.024	0.024	0.024
%Change Cl	1.03950104	0.21008403	0.21052632	0	0
%Change Cd	0	0	0	0	0

Figure 19: Data for Grid sensitivty

Drag conversion factor: 0.0748.

Lift conversion factor: 0.3952

Pitching conversion factor: 0.0108

Dynamic pressure was determined using:
$q[pa]=1.175*9.792*Betz[mmH2O]$

Aerodynamic coefficients of lift, drag and pitching-moment was obtained from these values:

$$Cl=\frac{L}{qS}$$

$$CD=\frac{D}{qS}$$

$$Cm=\frac{M}{qSCmac}-C_L\frac{Cpivot}{Cmac}$$

Wing area S = 0.214 m^2

Mean aerodynamic chord C_{mac} = 0.344

C_{pivot} = 0.444 m

$$K_P=\frac{dCL}{d\alpha}$$

$$K_I=\frac{dCD}{d\,C_L^2}$$

$$K_V=\frac{K_p-K_P^2*K_I}{\cos\Lambda_{¿}}$$

$$CL = K_p * \sin\alpha * (\cos\alpha)2 + KV * \sin\alpha * |\sin\alpha| * \cos\alpha$$
$$CD = CL * \tan\alpha$$

K_p = Pitching Moment Coefficient
K_i = Rolling moment Coefficient
K_v = Yawing moment Coefficient

α = Angle of Attack (from -10 to 26)
cos $\Lambda_{\frac{c}{4}}$ = root tip sweep angle (47.8 degrees)